Catalysis Science & Technology

ROYAL SOCIETY OF CHEMISTRY

COMMUNICATION

View Article Online
View Journal



Cite this: DOI: 10.1039/d5cy00260e

Received 4th March 2025,
Accepted 2nd February 2026

DOI: 10.1039/d5cy00260e

rsc.li/catalysis

# A first principle study of a model bimolecular nucleophilic substitution reaction promoted by an ammonium catalyst supported on oxidized carbon black

Maria Voccia, [a] Rosaria Schettini, [b] Maria Rosaria Acocella *[b] and Sergio Tosoni *[a]

**The adsorption of a tetraalkylammonium ion was simulated on various surface sites of oxidized carbon black (oCB). Next, we studied a model $S_N2$-type reaction between sodium thiocyanate and benzyl bromide. The role of the support in stabilizing the reaction intermediates *via* hydrogen bonds is proven to be the keyfactor, as well as the mediator effect of the quaternary ammonium ion. These findings shed light on the experiments reporting the high activity of ammonium-based catalysts supported on oCB in this type of reaction.**

Phase-transfer catalysis (PTC) represents an important research area that has flourished in the last decades both for industrial and academic research.[1] Generally, for reactions that occur in heterogeneous conditions at the interface of two immiscible phases, the use of a PTC is necessary to transfer the reactants from one phase (the aqueous layer) to another (the organic layer) allowing the reaction to take place (Fig. 1). By using PTC, mild conditions and simple operations can speed up the reaction rate, improve the selectivity, and enable the use of inexpensive and environmentally friendly reagents and solvents. Generally, onium salts such as quaternary ammonium[2–4] and phosphonium salts[5–7] have been demonstrated to be the catalysts of choice for organic reactions. Given their high solubility in water, however, their recovery, and recycling is limited when the reaction is carried out in aqueous media to reduce the use of polluting organic solvents.

Therefore, the immobilization of onium salts on a solid support provides a practical solution to separation, recovery and recycling processes reducing wastewater generation in accordance with some of the 12 principle of Green Chemistry.[8,9] Many approaches have been proposed to immobilize organic cations such as ammonium or phosphonium salts, like anchoring on polymer and clay supports,[10–13] porous solid catalysts,[14–16] and recently carbonaceous materials.[17,18]

Specifically, PTC catalysts based on carbon intercalation compounds were found to efficiently catalyse a nucleophilic substitution reaction performed both in a biphasic (liquid–liquid) system and, most interestingly, only in water, by using either ammonium or phosphonium cations. The new catalysts offer high conversion (up to 98%) and, given their heterogeneous nature, they can be recovered and recycled preserving their efficiency for various cycles of reaction. Intercalation compounds with either ammonium or phosphonium cations are synthesized by simple processes, such as alkaline treatment in solution or by mechanochemical reactions.[1] The catalysts can be easily obtained starting from a highly disordered oxidized carbon black (oCB) support. The alkaline treatment of the oCB dispersion in water can provide the replacement of metal ions with ammonium ions (*e.g.* dihydrogenated tallow dimethyl ammonium ion, 2HT) on graphitic layers, affording an ordered intercalate crystalline structure with long tails perpendicular to the graphite layer. The interaction among the alkyl chains generates an additional ordered phase named hexagonal rotator phase,[17] as reported in Fig. 2. Seeking for a rationalization in the complex design of PCT catalysts, we hereby elucidate through computational modelling the mechanism of action of our recently reported PTC carbonaceous-based material. According to our recent papers, this catalyst has been shown to be effective in

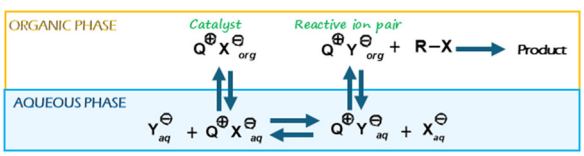


Fig. 1 Schematic representation of phase-transfer catalysis.

[a] Department of Materials Science, University of Milan-Bicocca, Via Roberto Cozzi 55, 20125, Milan, Italy. E-mail: sergio.tosoni@unimib.it
[b] Department of Chemistry and Biology "A. Zambelli", University of Salerno, Via Giovanni Paolo II, 132, 84084, Fisciano (Sa), Italy

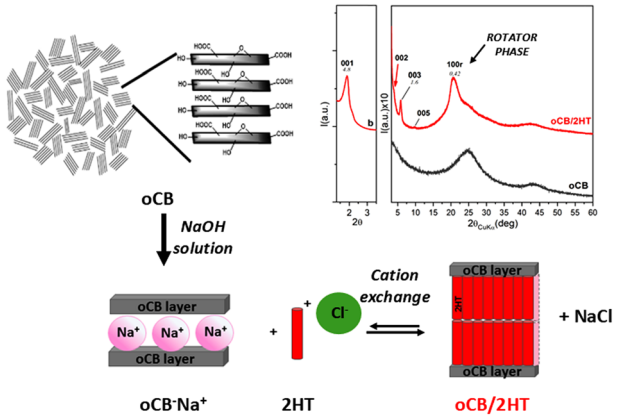


Fig. 2 A schematic representation of the oCB/2HT catalyst preparation.

nucleophilic substitutions not only in conventional biphasic systems, but also in aqueous solutions, with conversion up to 95%, with an easy recycle and reuse with no decrease in efficiency (Fig. 3).[1,17,18]

Specifically, the reaction proceeds *via* cation exchange between oCB/2HT and NaSCN, generating the 2HT/SCN ionic pair. This pair migrates to the organic substrate interface, where the $S_N2$ nucleophilic substitution occurs. The resulting 2HT/Cl subsequently reacts with the sodium intercalation compound, regenerating oCB/2HT. In this work, we will focus exclusively on a model of carbon-based material obtained by the adsorption of ammonium ions on an oxidized carbon black layer. This model focuses on the role of the $N(CH_3)_4^+$/oCB interface in the reaction, neglecting, for simplicity, the presence of the long alkyl chains which leads to the formation of the rotator phase (Fig. 2).

Particular attention is devoted to unravelling the role of the support as well as the effect of the quaternary ammonium salt, by simulating the reaction on a rich functionalized carbon black layer. In recent years, the DFT approach was proven to be successful in understanding the electronic properties and functionalities of graphene oxide (GO), reduced graphene oxide (rGO)[19–22] and graphite oxide,[23] as well as the adsorption of various species (including gases and metal ions) on the surface of these

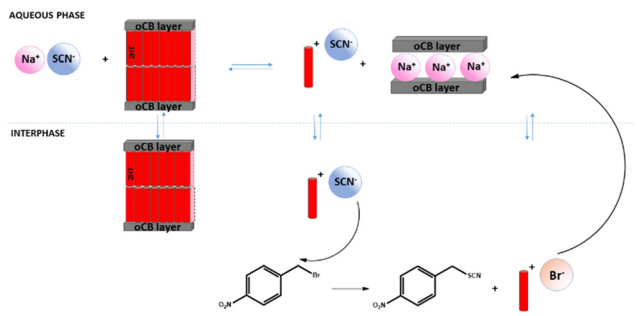


Fig. 3 Possible pathway of cation release exerted by oCB/2HT in the $S_N2$ reaction of nitro-benzyl bromide by NaSCN.

materials.[24,25] It must be stated, moreover, that complex interfaces involving GO layers have been described, but recurring to semiempirical methods and molecular mechanics.[26–28] At variance from GO and rGO, the computational models of oCB in the literature exhibit a smaller concentration of oxygen-containing functional groups. In detail, the study of Zhou[29] provides a comprehensive understanding of how Na and Ca catalyze coal gasification by integrating DFT calculations with experimental results. The oxidized carbon black sheet as a simplified coal model with three condensed rings as aromatic hydrocarbons, functionalized by one hydroxyl group has been used in that study.[29] Instead, the study of Sherazi integrates DFT simulations with experimental validation to design and evaluate oCB materials for the electrochemical detection of arsenic (As) in aqueous solutions, adopting two combined epoxy groups at the carbon sheet as representative of oxidized carbon black.[30] The extreme simplicity of the structural models of oCB adopted in the aforementioned studies does not fully align with several experiments conducted with different techniques (*i.e.* TGA, DSC, X-ray diffraction and elemental analysis), where it has been possible to structurally characterize the oxidized carbon black materials,[31] defining which functional groups are present, the degree of aromaticity as well as the thickness of the layer and the disorder among the layers. The outcome of these experimental studies, thus, reveals the highly complex structure of oCB, and the only partial adequacy of the previous computational models. This article aims first at bridging this gap. In the first part of the paper, structural studies on oxidized carbon black models with several functional groups as well as aromatic, hydrocarbons and heteroatomic rings were reported. In the second part, the formation of the oCB/ammonium ion[32] adduct as catalytic system and the study of the mechanism for the nucleophilic substitution reaction $S_N2$ of NaSCN with benzyl bromide was considered on the most stable model that we obtained. In some recent experimental work,[1,17] a cation exchange between oCB/2HT and NaSCN was hypothesized, thereby yielding the $2HT^+/SCN^-$ ion pair. A nucleophilic substitution reaction would then take place between the new ionic pair and the organic substrate once they reach the interface. The resulting $2HT^+/Br^-$ yields once more the oCB/2HT, after reacting with the sodium intercalation compound. In order to shed light on the mechanistic aspects of the reaction, we hereby discuss a simplified catalytic scheme, where NaSCN first adsorbs on an $N(CH_3)_4^+$/oCB layer, and then reacts with an organic substrate, namely benzyl bromide. The results presented here are thus directly relevant to understand the results of the recent experiments and drive further experimental studies. In the present study, all first-principle calculations were conducted within the framework of spin-polarized DFT calculations,[33,34] as implemented in the Vienna *Ab initio* Simulation Package (VASP), for more details see SI.[35–38] For implicit solvation calculations, we used VASPsol++,[39] a software package that incorporates solvation

into VASP within a self consistent dielectric continuum model. The relative permittivity was set to 80 mimicking the aqueous environment.

The adsorption free energy of reactants, intermediates and products are defined as:

$$\Delta G_{ads} = \Delta G_{Mol/oCB} - \Delta G_{Mol} - \Delta G_{oCB} \quad (1)$$

where $\Delta G_{Mol/oCB}$ represent the free energy of the examined adduct, $\Delta G_{Mol}$ and $\Delta G_{oCB}$ denote the free energies of solvent-phase adsorbates and oCB sheet, respectively. The effect of the solvent is accounted for in all cases.

## Structural optimization of oCB layer

The optimized structure of oxidized carbon black is presented in Fig. 4(a and b) (top view) and (c) (side view). This structure was derived from a single layered graphene-like sheet, consisting of fifty-one carbon atoms. Different guess structures have been prepared, with oxygen/carbon weight ratio (O/C) gradually increased from 0.02 to 0.46. The oxidation of graphene to carbon black by replacing carbon atoms with oxygen atoms and by introducing additional oxygen atoms can induce the formation of many different oxygen-containing functional groups such as ether, epoxy, hydroxyl, and carbonyl groups. Oxygen can also replace carbon within the oxidized graphitic sheet, forming various aromatic and saturated rings and heterocycles, with isolated or even conjugated double bonds. These findings are in line with the experimental results, where it is shown that, on oCB, dehydration and decarboxylation reactions conducted at high temperature lead to isolated or even conjugated double bonds, whereas for GO and eGO (exfoliate graphene oxide) these reactions can lead to aromatization (*e.g.* benzene like structure).[31] This complexity is indeed a great challenge for modelling, also considering that the models of oxidized carbon black presented in the literature are often quite simple, only bearing one or two of the functional groups, as mentioned above.[29,30] In this work, after several trials (that failed leading to structures with unsaturated bonds, or non-realistic three-membered rings), we obtained a doped sheet with an O/C weight ratio of 0.46, including the presence of all main oxidated functional groups (–ROR, –ROH, –RCOOH, –RCOOR, *etc.*), and displaying no dangling bonds or strained rings. This model abides to the main structural features of oxidized graphene described in the paper from Lerf *et al.*:[40] oxygen-containing functional groups are grafted on both sides of the graphitic layers, and their distribution abides to the principle of avoiding exceeding steric hindrance (no more than five substituents per six-membered rings). The absence of dangling bonds in the model ensures that no spurious highly reactive centers are introduced in the structure. It must be stated, however, that the presence of intrinsic paramagnetic centers in GO seems to suggest that some unsaturated bonds are indeed present.[41] The layer consists of eight hydrogen atoms, thirty-six carbon atoms and seventeen oxygen atoms. In agreement with the experimental results,[31] a layer thickness of about 5.5 Å was obtained due to the presence of different functional groups which also induces a change in the carbon atoms hybridization, that in turn induces the layer buckling. At first the structure of the selected oCB layer has been fully relaxed with PBE, then, its stability at room temperature has been checked recurring to *Ab Initio* Molecular Dynamics calculations (AIMD), gradually increasing the temperature from 0 K to 100 K, 200 K and 300 K, with trajectories of 1 ps. The thermal energy fluctuations (Fig. 4A–C) indicate that no phase transitions take place, ensuring the thermal stability of our model. The time span of the AIMD simulations is limited by the relatively high cost of these calculations, but the absence of any feature indicating significant structural rearrangements is noteworthy. The right panel of the figure provides side views of the examined systems, revealing that the oxidized layer exhibits no discernible structural reorganization or disintegration up to room temperature. This observation underscores the robustness of the structure under investigation, suggesting that it maintains its integrity under the influence of a typical annealing temperature. One must clearly state that the model presented here is not the true and only possible oCB structure, but the presence of several representative functional groups, the realistic O/C ratio and the thermal stability at room temperatures are

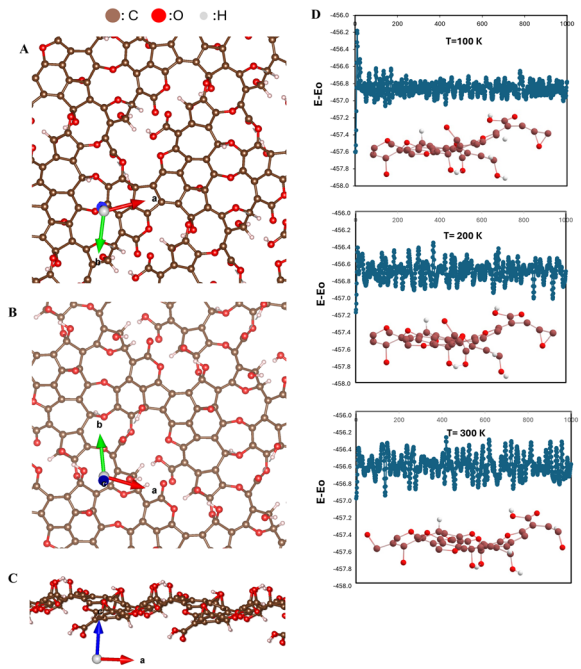


**Fig. 4** The optimized oCB structure from both top (A and B) and side views (C) (gray atoms represent carbon, red atoms represent oxygen and light gray atom represent hydrogen). (D) Variations in the gradient values of the total energies for the single oCB layer as a function of simulation time at the three different temperatures. The insets show the final atomic arrangements captured at the end of the simulation. $E_0$ denotes the total energies of the system at 0 K and $E$ the total energies at 100 or 200 or 300 K, respectively.

features highlighting its reliability to further studies adsorption and chemical reactions. It must be stated that room temperature is realistic with respect to the typical use of this oxidized sheet[31] as deposition protocols of oCB, as well as it was done in studies of organic reactions that shows oCB as activator or catalyst.[1,17,18]

## Adsorption of tetramethyl ammonium chloride ($N(CH_3)_4^+Cl^-$)

For simplicity, tetramethyl ammonium chloride was chosen as a model of ammonium ion, to provide mechanistic insights for the comprehension of the PTC reaction on a heterogenous carbon-based catalytic system, *i.e.* oCB/2HT adduct. The adoption of this simplified model of the catalyst was supported by the experimental study conducted by some of us, which reports comparable high activity for oCB and tetraalkylammonium salts commonly used as phase-transfer catalysts.[17] Moreover, some test calculations[32] on oCB/2HT adduct (for more details see SI) show that the interaction of the ammonium cation with oCB is only marginally affected by the presence of the active chain (Fig. S3 and Table S4).

We simulated the aqueous environment using a self consistent continuum solvation approach within VASPsol++ and the water as solvent of PCM model. The results in vacuum are reported, for comparison, in the SI, Fig. S4. Furthermore, Tables S1–S3 summarize the free energy of solvation ($\Delta G_{sol}$) for all the species involved.

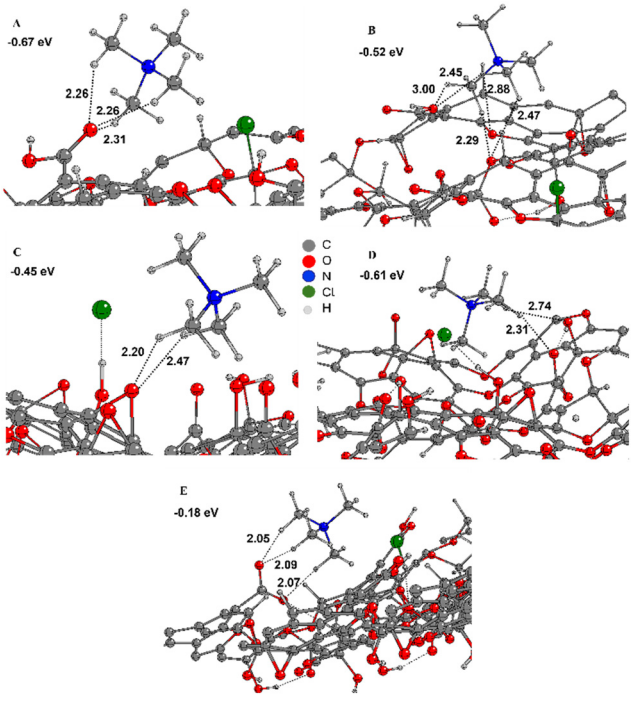


**Fig. 5** Optimized atomic structures for the initial intermediate of $N(CH_3)_4^+$ ion in various configurations (A–E) on oCB. The energy costs of the adduct $N(CH_3)_4^+$/oCB/$Cl^-$ formation are reported in eV. The distances are reported in Å.

To study the adhesion strength of the ammonium ion on the various oCB surface sites, *i.e.* its functional groups, a 2 × 2 supercell was build starting from the initial cell parameters of the oCB layer. The supercell size is 22.978 Å × 23.351 Å × 42.206 Å and the density of tetramethyl ammonium chloride is 0.19 molecules per $nm^2$. In Fig. 5A the strongest possible interaction of $N(CH_3)_4^+$ with carboxylic acid group is reported, with adsorption free energies of −0.67 eV. In Fig. 5B it is shown a structure where the ammonium group interacts with ether groups, with an adsorption energy of −0.52 eV. Finally, also the interaction of $N(CH_3)_4^+$ with epoxide and ester groups in Fig. 5C and D, respectively, have been obtained, with free adsorption energies almost close to the carboxylic case.

Despite the restricted difference of only 0.1–0.2 eV for the energies of these adducts, the strongest interaction was found between the carboxylic acid and the $N(CH_3)_4^+$ ion, as reported in Fig. 5A, with several short distances related to hydrogen bonds between the $N(CH_3)_4^+$ and the carboxylic acid group, in agreement with the experimental results.[1,17] This different behavior can be ascribed to the stronger propensity of carboxylic acid to share its electron doublet with hydrogen atoms than the other oxygen based functional groups. A more detailed Fig. S1 is reported in the SI. In conclusion, the adduct $N(CH_3)_4^+$/oCB/$Cl^-$ exhibits preferential interaction through a hydrogen bond between $N(CH_3)_4^+$ and the carboxylic acid functional group, supporting the spectroscopic evidence for the shift of carboxyl group frequency from 1715 $cm^{-1}$ in oCB to 1640 $cm^{-1}$ in oCB/2HT with the carboxylate group formation, that thus interacts with 2HT species preferentially.[17] In details, it was reported that a cation exchange between $Na^+$ and $N(CH_3)_4^+$ can be obtained after alkaline treatment of oCB dispersion in water and NaOH. Thus, it is reasonable to assume that the deprotonated carboxylate species of oCB coordinates stronger the $N(CH_3)_4^+$ ion[17] than the carboxylic acid one. However, in the computational model, the explicit inclusion of the $H^+$ ion on the carboxylate functional groups is necessary to ensure the neutrality of the supercell. This could explain the very similar adsorption energies among the reported adducts in Fig. 5.

To prove the strongest interaction, one deprotonated carboxylate species on oCB was simulated favoring the electrostatic interaction between the $Cl^-$ and $H^+$ ion on the surface and confirming the strongest interaction as reported in Fig. 5E, for more detail see Fig. S2.

Although, the ionic interactions have been confirmed with short alkyl chain ammonium ion, in the presence of substituent with long alkyl chains, additional interchain interactions should be considered, possibly influencing the oCB/2HT stability as well as its catalytic behavior. This aspect, thus, also was investigated, proving that a simple truncation of the alkyl chains does not influence the interaction of the ammonium moiety with oCB (the strongest interactions are detected between the hydrogen atoms of the alkyl groups directly connected to the nitrogen atom) and (ii)

including a single complete alkyl ammonium fragment in the simulation does not lead to a more realistic structure at the solid state, which would probably require several alkyl ammonium moieties binding two oCB layers (*i.e.* the real system, which is not feasible at the state of the art).[17,18] For more details see Fig. S3.

## $S_N2$ reaction mechanism

To understand the potential of our oCB layer model, we have tested a simple $S_N2$ reaction between the benzyl-bromide and sodium thiocyanate as it is the first example reported two years ago in which the oCB/2HT system (with a O/C weight ratio of 0.58) is used as catalyst of PTC process for this reaction.[1,17] To simplify our model, as previously mentioned, explicit inclusion of the $H^+$ ions on the carboxylate groups was used to ensure the neutrality of the supercell.

All the binding energies are computed with respect to the clean oCB, as starting point of reaction, and to the molecules at infinite distance and in aqueous environment.

We hypothesize a catalytic cycle where, at first, the ammonium ion is physically adsorbed on oCB with an adsorption energy $\Delta G_{ads}$ of −0.67 eV. The location of the ammonium ion, as already mentioned, is preferentially close to carboxylic acid, *via* O···HN hydrogen bonds with distances of 2.26 and 2.31 Å, whereas the chloride ion is far from the ammonium one, interacting with a carbon atom, Fig. 6A. The adduct represents the starting point of our catalytic system for this reaction. Indeed, some of us have reported that the reaction of 4-nitrobenzylbromide in the presence of NaSCN provides the product 4-nitrobenzylthiocyanate with 98% conversion in 4 h, while in the presence of oCB without 2HT the same reaction proceeds with 8% in 24 h and only with 2HT the reaction requires 24 h to reach up to 89% yield, showing the better efficiency of oCB/2HT adduct as catalyst.[17] Next, a cationic exchange reaction takes place: sodium thiocyanate releases a $Na^+$ cation, which is stabilized close to the surface due to favorable electrostatic interactions, rather than being tightly bound to a specific surface site, while the ammonium ion binds to the thiocyanate species, leaving the –RCOOH surface site, see Fig. 6B (in detail, the Na–S distance in sodium thiocyanate is stretched from to 2.41 Å to 2.73 Å upon binding to oCB, highlighting the role of the support in activating the reactant).

This step is thermodynamically favorable with a binding energy of −0.89 eV with respect to clean oCB and reactants at infinite distance. This step, thus, is exergonic by almost 0.20 eV, in agreement with the electrostatic nature of the stabilizing interactions. Next, the benzyl bromide molecule ($C_6H_5CH_2Br$ in Fig. 6C) is co-adsorbed physically on the oCB

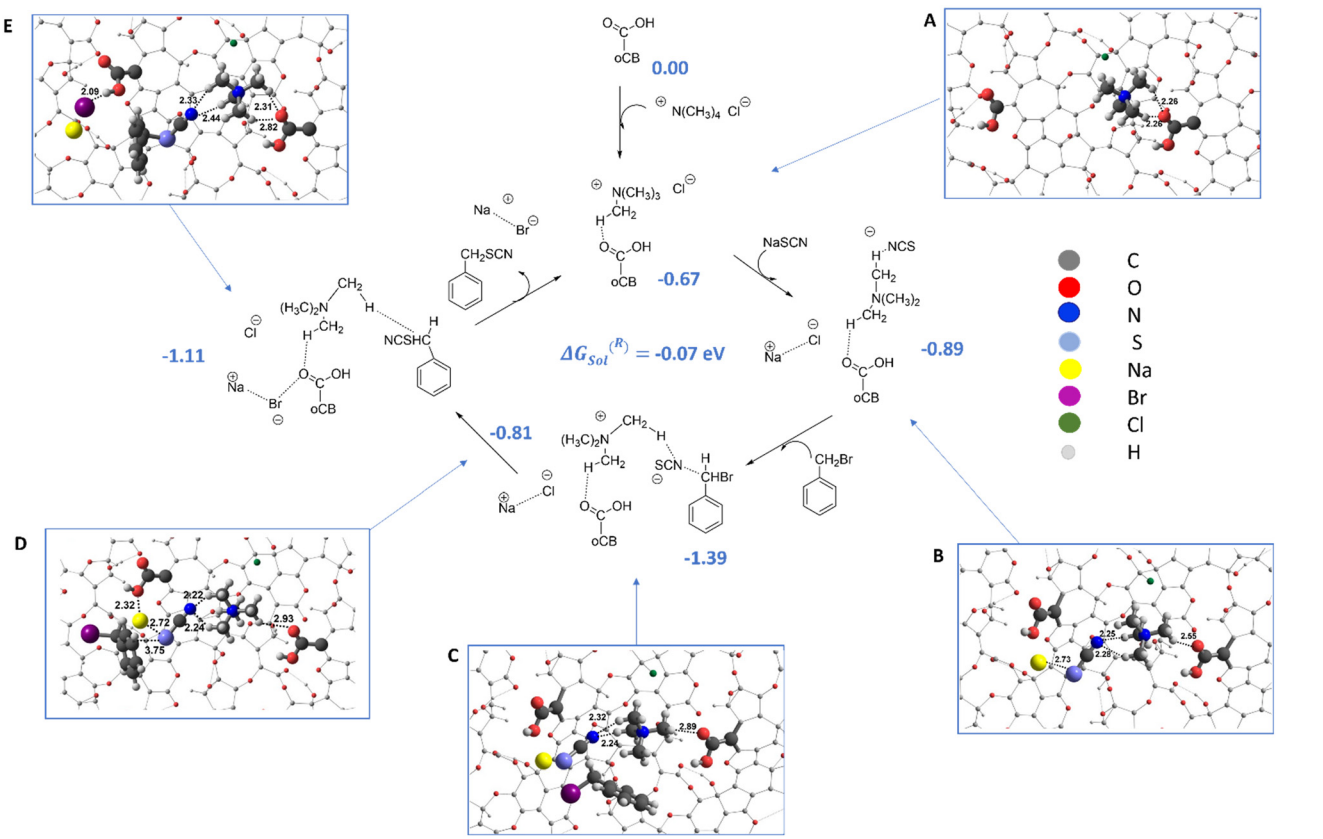


**Fig. 6** DFT-calculated $S_N2$ substitution nucleophilic reaction. The inset shows the structure of each intermediate. The labelling A–E refers to the subsequent reaction steps. Binding energy variations are reported in eV for each step, (gray atoms represent carbon, red atoms represent oxygen, cyan represent sulfur atoms, yellow represents sodium atoms magenta represent bromine atoms, green represent chloride atoms and light gray atom represent hydrogen atoms).

layer, by a lone pair of one oxygen atom of the oCB interacting with the hydrogen atoms of the aryl ring, with a binding energy of −1.39 eV. This step, thus, is as well exergonic by 0.52 eV. The presence of the benzyl bromide determines a change in the orientation of the thiocyanate ion toward the new molecule and the $N(CH_3)_4^+$ ion: the thiocyanate ion tightly interacts the $N(CH_3)_4^+$ ion *via* the N atom, whereas the S atom is very close to the organic molecule, *via* an intermediate that has an adsorption energy of only −0.81 eV (endergonic of almost 0.50 eV respect to the reactants), resembling a transient geometry between the reactants and the products, see Fig. 6D.

The reaction product, benzyl thiocyanate, is formed *via* the nucleophilic substitution reaction that takes place between the new ionic pair, *i.e.* $N(CH_3)_4^+$ cation and $SCN^-$ anion, and the organic molecule, $C_6H_5CH_2Br$. This structure has an adsorption energy of −1.11 eV with respect to oCB and reactants at infinite distance. This step, thus is exergonic, ensuring the feasibility of the reaction (Fig. 6E).

The bromide ion forms a strong hydrogen bond with a surface R–OH group, stabilizing the adduct, see Fig. 6E. The resulting $N(CH_3)_4^+/Br^-$ yields once more the starting oCB/$N(CH_3)_4^+$ adduct, after reacting with the sodium intercalation compound and loss of a NaBr and $C_6H_5CH_2$-SCN molecule with a barrier of almost 0.50 eV for the release of the products. The heterogeneous nature of the catalyst, and its easy recovery by extraction with ethyl acetate, drives the reaction toward the desired product while allowing efficient separation of the adduct from the aqueous phase. This pathway is in line with the proposed mechanism already reported.[17,18] Overall, the reaction is exergonic ($\Delta G$ = −0.07 eV, Fig. 6).

## Role of $N(CH_3)_4Cl$

In details, we report that the ammonium salt effectively acts as a mediator between the species hosted in the two phases. At first, the addition of the NaSCN molecule to the adduct determines the cation exchange yielding the $N(CH_3)_4^+/SCN^-$ ionic pair (with two new strong interactions established at distances N···H of 2.25 and 2.28 Å) as reported in Fig. 6B. This, in turns, slightly increases the distance of $N(CH_3)_4^+$ ion from the carboxyl acid group on oCB (2.55 Å *vs.* 2.26 Å). The possible interaction between the $N(CH_3)_4Cl$ and benzyl-bromide was as well simulated, but resulted strongly unfavorable (only −0.15 eV with respect to the reference reactants). Next, benzyl bromide displaces the tetramethylammonium ion from the oCB carboxylic site, Fig. 6C and D. The interaction between the nucleophilic benzyl bromide and NaSCN with the $N(CH_3)_4^+$ ion is prodrome to the $S_N2$ reaction, followed by the displacement of the product. The interaction of the tetramethylammonium ion with the –COOH site on oCB is then restored. The bromide ion is stabilized on another nearby –COOH site on oCB, see Fig. 6E.

## Conclusion

For the first time, a new computational model to describe the surface of oxidized carbon black has been reported. It is important to emphasize that inclusion of multiple representative functional groups, a good agreement with the observed O/C ratio, and thermal stability at room temperature underscores its validity. Moreover, mechanistic details of the surface reaction chemistry that confirms the experimental behaviour were identified proving that: (i) the strong interaction of the $N(CH_3)_4^+$ ion as model of the 2HT molecule is useful for understanding the mechanism of nucleophilic substitution reaction; (ii) the role of intermolecular interactions at the interface with the oCB support seems to be very important in driving the reaction; (iii) the role of quaternary ammonium salt as mediator for this PTC reaction.

Therefore, these findings clarify both the chemical process and the importance of surface modeling choices for future developments in the field. Starting from these insights which pave the way for developing new catalytic systems, further investigations are currently undergoing using functionalized carbon black surfaces with other adsorbate molecules[29] and organic reactions[42–49] as well as the solid electrolyte interphase interactions with carbonaceous anode materials.[50–52]

## Conflicts of interest

There are no conflicts to declare.

## Data availability

The data supporting this article have been included as part of the supplementary information (SI). Supplementary information is available. See DOI: https://doi.org/10.1039/d5cy00260e.

## Acknowledgements

Ministero dell'Università e della Ricerca is gratefully acknowledged. MV and ST acknowledge financial support from Fondazione Cariplo, grant 2022-0713 PLANET ("Photocatalytic recovery of iodine from iodinated waste using single-atom catalysts"), and the support of CINECA for computational resources *via* the ISCRA initiative.

## References

1 R. Schettini and M. R. Acocella, *ChemCatChem*, 2024, e202301425.
2 C. M. Starks, C. L. Liotta and M. Halpern, *Phase-transfer catalysis: fundamentals, applications and industrial perspectives*, Chapman & Hall, New York, 1994.
3 T. Kanemitsu, M. Sato, M. Yoshida, E. Ozasa, M. Miyazaki, Y. Odanaka, K. Nagata and T. Itoh, *Org. Lett.*, 2016, **18**, 5484.
4 X. Yang, Y. Deng, D. Ling, T. Li, L. Chen and Z. Jin, *ACS Catal.*, 2025, **15**, 1973–2001.

 

5 A. K. Ghosh and K. A. Hussain, *Tetrahedron Lett.*, 1998, **39**, 1881–1884.
6 T. Werner, *Organocatal.*, 2009, **351**, 1469–1481.
7 D. Enders and T. V. Nguyen, *Org. Biomol. Chem.*, 2012, **10**, 5327–5331.
8 P. T. Anastas and J. C. Warner, *Green chemistry: theory and practice*, Oxford University Press, Oxford, 1998.
9 P. Anastas and N. Eghbali, *Chem. Soc. Rev.*, 2010, **39**, 301.
10 R. Annunziata, M. Benaglia, M. Cinquini, F. Cozzi and G. Tocco, *Org. Lett.*, 2000, **2**, 1737.
11 S. Desikan and L. K. Doraiswamy, *Chem. Eng. Sci.*, 2000, **55**, 6119.
12 E. Murugan and P. Gopinath, *Appl. Catal., A*, 2007, **319**, 72.
13 H. Peng, M. Lei, L. Yang, J. Sun, L. Yang and Q. Zhao, *ACS Omega*, 2020, **5**, 21468.
14 S. Dasgupta and B. Torok, *Org. Prep. Proced. Int.*, 2008, **40**, 1.
15 B. Song, L. Guo, R. Zhang, X. Zhao, H. Gan, C. Chen, J. Chen, W. Zhu and Z. Hou, *J. CO2 Util.*, 2014, **6**, 62.
16 X.-L. Shi, Y. Chen, Q. Hu, H. Meng and P. Duan, *Ind. Eng. Chem. Res.*, 2018, **57**, 7450.
17 A. Melillo, A. Kiani, R. Schettini and M. R. Acocella, *Mol. Catal.*, 2023, **537**, 112951.
18 A. Kiani, D. Coscia, R. Schettini and M. R. Acocella, *Mol. Catal.*, 2023, **550**, 113558.
19 P. Suvarnaphaet and S. Pechprasarn, *Sensors*, 2017, **17**, 10.
20 Q. Fatima, H. Zhang, A. A. Haidry, R. Hussain, R. A. Alshgari and S. Mohammad, *Diamond Relat. Mater.*, 2024, **146**, 111151.
21 E. V. Gómez, N. A. R. Guarnizo, J. D. Perea, A. S. López and J. J. Prías-Barragán, *ACS Omega*, 2022, **7**(5), 3872–3880.
22 N. Maslekar, P. B. Zetterlund, P. V. Kumar and V. Agarwal, *ACS Appl. Nano Mater.*, 2021, **4**(3), 3232–3240.
23 D. W. Boukhvalov and M. I. Katsnelso, *J. Am. Chem. Soc.*, 2008, **130**(32), 10697–10701.
24 S. Thompho, T. Rungrotmongkol, O. Saengsawang and S. Hannongbua, *J. Sci. Technol.*, 2017, **39**, 6.
25 J. N. Tiwari, K. C. Kemp, J. A. Perman, A. B. Bourlinos, K. S. Kim and R. Zboril, *Chem. Rev.*, 2016, **116**, 9.
26 H. Tang, Y. Zhao, S. Shan, X. Yang, D. Liu, F. Cui and B. Xing, *Environ. Sci. Technol.*, 2018, **52**, 7689.
27 W. Li, X. Zheng, Z. Dong, C. Li, W. Wang, Y. Yan and J. Zhang, *J. Phys. Chem. C*, 2016, **120**, 26061.
28 P. R. Reddy, K. Anki Reddy and A. Kumar, *J. Phys. Chem. B*, 2024, **128**, 5218.
29 R. Bai, L. Liu, N. Li, Q. Liu, Y. Meng, Y. Teng, H. Zhou and X. Zhou, *Fuel*, 2023, **349**, 128654.
30 A. Batool, S. Qureshi, A. Ahmad, S. Zubaid, L. Saeed, K. Ayub, T. Rasheed and T. A. Sherazi, *Surf. Interfaces*, 2024, **52**, 104843.
31 M. Maggio, M. R. Acocella and G. Guerra, *RSC Adv.*, 2016, **6**, 105565.
32 M. Tomasini, M. Voccia, L. Caporaso, M. Szostak and A. Poater, *Chem. Sci.*, 2024, **15**, 13405–13414.
33 W. Kohn and L. Sham, *Phys. Rev. [Sect.] A*, 1965, **140**, A1133.
34 P. Hohenberg and W. Kohn, *Phys. Rev. [Sect.] B*, 1964, **136**, B864.
35 G. Kresse and J. Hafner, *Phys. Rev. B: Condens. Matter Mater. Phys.*, 1993, **47**, 558.
36 G. Kresse and J. Hafner, *Phys. Rev. B: Condens. Matter Mater. Phys.*, 1994, **49**, 14251.
37 G. Kresse and J. Furthmüller, *Comput. Mater. Sci.*, 1996, **6**, 15–50.
38 G. Kresse and J. Furthmüller, *Phys. Rev. B: Condens. Matter Mater. Phys.*, 1996, **54**, 11169.
39 K. Mathew, R. Sundararaman, K. Letchworth-Weaver, T. A. Arias and R. G. Hennig, *J. Chem. Phys.*, 2014, 140.
40 (*a*) S. M. R. Islam, F. Khezeli, S. Ringe and C. Plaisance, *J. Chem. Phys.*, 2023, **159**, 234117; (*b*) A. Lerf, H. He, M. Forster and J. Klinowski, *J. Phys. Chem. B*, 1998, **102**, 4477–4482.
41 G. De Thomasis, A. Galante, G. Fioravanti, L. Ottaviano, M. Alecci and G. Profeta, *J. Chem. Phys.*, 2023, **158**, 124709.
42 W. Xiao, Q. Sun, J. Liu, J. Liu, B. Xiao, P.-A. Glans, J. Li, R. Li, J. Guo, W. Yang, T.-K. Sham and X. Sun, *Nano Res.*, 2017, **10**, 4378–4387.
43 N. Dimakis, I. Salas, L. Gonzalez, O. Vadodaria, K. Ruiz and M. I. Bhatti, *Molecules*, 2019, **24**, 754.
44 G. AlJaber, B. AlShammari and B. AlOtaibi, *Nanomaterials*, 2025, **15**, 992.
45 B. C. Arnold, E. d. S. Machado, J. B. L. Martins, L. G. Paterno and J. R. S. Politi, *J. Phys. Chem. C*, 2025, **129**, 7879–7893.
46 M. J. Saadh, A. Kumar, D. Bhanot, J. Makasana, H. Hassan, B. Kumari, G. V. S. Prasad, M. Hussen and A. A. Almehizia, *Phys. B*, 2025, **698**, 416756.
47 A. Kiani, M. R. Acocella, V. Granata, E. Mazzotta, C. Malitesta and G. Guerra, *ACS Sustainable Chem. Eng.*, 2022, **10**, 16019–16026.
48 M. R. Acocella, M. De Pascale, M. Maggio and G. Guerra, *J. Mol. Catal. A: Chem.*, 2015, **408**, 237–241.
49 A. Kiani, M. Naddeo, F. Santulli, V. Volpe, M. Mazzeo and M. R. Acocella, *Molecules*, 2025, **30**, 94.
50 S. Gravelle and L. Botto, *Langmuir*, 2021, **37**, 13322–13330.
51 W. Xiao, Q. Sun, J. Liu, B. Xiao, P.-A. Glans, J. Li, R. Li, J. Guo, W. Yang, T.-K. Sham and X. Sun, *Nano Res.*, 2017, **10**, 4378–4387.
52 S. J. An, J. Li, C. Daniel, D. Mohanty, S. Nagpure and D. L. Wood III, *Carbon*, 2016, **105**, 52–76.